



ARTICLE

## Research on Rosewood Micro Image Classification Method Based on Feature Fusion and ELM

Xiaoxia Yang<sup>1</sup>, Yisheng Gao<sup>2,\*</sup>, Shuhua Zhang<sup>1</sup>, Zhedong Ge<sup>1</sup> and Yucheng Zhou<sup>1</sup>

<sup>1</sup>School of Information and Electrical Engineering, Shandong Jianzhu University, Jinan, 250101, China

<sup>2</sup>School of Architecture and Urban Planning, Shandong Jianzhu University, Jinan, 250101, China

\*Corresponding Author: Yisheng Gao. Email: gao\_sdjz@126.com

Received: 03 March 2022 Accepted: 02 April 2022

### ABSTRACT

Rosewood is a kind of high-quality and precious wood in China. The correct identification of rosewood species is of great significance to the import and export trade and species identification of furniture materials. In this paper, micro CT was used to obtain the micro images of cross sections, radial sections and tangential sections of 24 kinds of rosewood, and the data sets were constructed. PCA method was used to reduce the dimension of four features including logical binary pattern, local configuration pattern, rotation invariant LBP, uniform LBP. These four features and one feature not reducing dimension (rotation invariant uniform LBP) was fused with Gray Level Co-Occurrence Matrix and Tamura features, respectively, a total of five fused features  $LBP+GLCM+Tamura$ ,  $LCP+GLCM+Tamura$ ,  $LBP_{P,R}^{u2}+GLCM+Tamura$ ,  $LBP_{P,R}^{ri}+GLCM+Tamura$  and  $LBP_{P,R}^{riu2}+GLCM+Tamura$  were obtained. The five fused features were classified by extreme learning machine and BP neural network. The classification effect of feature  $LBP_{P,R}^{u2}+GLCM+Tamura$  combined with extreme learning machine was the best, and the classification accuracy of cross, radial and tangential sections reached 100%, 97.63% and 94.72%, respectively, which is 0.83%, 2.77% and 5.70% higher than that of BP neural network. The classification running time of ELM is less than 1 s, and the classification efficiency is high. In conclusion, the  $LBP_{P,R}^{u2}+GLCM+Tamura$  method combined with extreme learning machine can be used as a quick and accurate classifier, providing an efficient and feasible classification method of rosewood.

### KEYWORDS

Rosewood; micro CT; feature fusion; ELM; BP neural network

## 1 Introduction

Wood, with the characteristics of ecological and environment-friendly, is an anisotropic biomass material. There are many kinds of wood, and there are great differences among different families and genera. The characteristics of similarity and difference appear in different wood in a family and genus. The category of wood is difficult to identify through macro structure, such as color, material and texture [1,2]. Experienced experts are needed for wood identification, according to the distribution of wood microstructure, such as vessel pores, wood rays and axial parenchyma in cross sections, radial sections and tangential sections [3–5]. Although this identification method is very effective, the standard of wood scientific knowledge and skills of personnel is highly required in order to realize wood classification



[6,7]. Comparing with traditional anatomical methods, a micro CT was used to collect the images of cross sections, radial sections and tangential sections of wood, and thousands of wood images were generated efficiently in a short time.

Some specific features of the micro images of wood were extracted for feature fusion, which were combined with ELM (Extreme Learning Machine) classifier to realize the rapid recognition of wood through cross section, radial section and tangential section. The method of feature fusion could combine the advantages of different features to improve the classification accuracy [8,9]. Ahmad et al. [10] applied the method of deep feature fusion to waste classification to obtain high classification accuracy. Zhao et al. [11] fused the characteristics of wood texture and spectrum, and BP neural network was used for wood classification, with a correct rate of 90%. After the fusion of texture and near-infrared spectral features, SVM (Support Vector Machine) was adopted by Wang et al. [12]. The accuracy could reach 100% without interference, and the classification accuracy was better than the traditional algorithm in the case of image distortion. The above feature fusion methods were based on spectral images, but a variety of texture features were extracted, fused and classified from micro images in this paper.

ELM, as a single hidden layer feedforward neural network algorithm, was widely used in image classification [13,14], data label classification [15], fingerprint classification [16] and other fields, with good learning efficiency and generalization performance. Xiao et al. [17] classified 180 samples of 6 kinds of construction waste obtained by hyperspectral technology, and the accuracy of ELM can reach 100%, showing a strong classification ability. Yang et al. [18] extracted the data characteristics of wood defects and used the ELM for classification. The accuracy rate reached 96.72% within 187 ms. Some researchers [19,20] used ELM to classify the spectral images of wood, and the classification accuracy reached more than 97%. Xiang et al. [21] proposed a wood classification algorithm based on LBP-DEELM (Local Binary Pattern-DE-ELM) model, which has better classification accuracy than BP neural network and SVM algorithm.

In this paper, the PCA (Principal Component Analysis) method was used to reduce the dimension of four features logical binary pattern (*LBP*), local configuration pattern (*LCP*), rotation invariant LBP ( $LBP_{P,R}^r$ ), uniform LBP ( $LBP_{P,R}^{u2}$ ) and one original feature ( $LBP_{P,R}^{riu2}$ ) was respectively fused with *GLCM* and *Tamura* features respectively, a total of five fused features  $LBP+GLCM+Tamura$  ( $LBP+G+T$ ),  $LCP+GLCM+Tamura$  ( $LCP+G+T$ ),  $LBP_{P,R}^{u2}+GLCM+Tamura$  ( $LBP_{P,R}^{u2}+G+T$ ),  $LBP_{P,R}^r+GLCM+Tamura$  ( $LBP_{P,R}^r+G+T$ ) and  $LBP_{P,R}^{riu2}+GLCM+Tamura$  ( $LBP_{P,R}^{riu2}+G+T$ ) were obtained. Using ELM and BP neural network methods, five fused features were classified.  $LBP_{P,R}^{u2}+G+T$  method showed excellent classification performance with ELM and BP neural network classification.

## 2 Materials and Dataset

### 2.1 Experimental Materials

According to the rosewood standard formulated by China in 2017, rosewood is divided into 29 species. This paper takes 24 species of rosewood as the research objects from 3 families (Papilionaceae, Ebenaceae, Caesalpiniaceae) and 5 genera (Pterocarpus, Dalbergia, Millettia, Senna, Diospyros). Among them, Pterocarpus includes 4 species: *Pterocarpus santalinus* L.f., *Pterocarpus erinaceus*, *Pterocarpus indicus* and *Pterocarpus macrocarpus*. Dalbergia includes 13 species: *Dalbergia odorifera* T. Chen, *Dalbergia cultrata*, *Dalbergia latifolia*, *Dalbergia louvelii* R.Vig, *Dalbergia melanoxydon*, *Dalbergia stevensonii* Standl, *Dalbergia bariensis* Pierre, *Dalbergia cearensis* Ducke, *Dalbergia cochinchinensis* Pierre, *Dalbergia frutescens* Var.tomentosa (Vogel) Benth, *Dalbergia granadillo* Pittier, *Dalbergia oliveri* Prain, *Dalbergia retusa* Hemsl. Millettia includes 2 species: *Millettia laurenii* De Wild, *Millettia leucantha*. Senna includes 1 species: *senna siamea*. Diospyros includes 4 species: *Diospyros* sp., *Diospyros crassiflora*, *Diospyros celebica*, *Diospyros* sp. The Latin names of 24 kinds of rosewood, the types of vessel pores, family names and origin information were given in Table 1. The experimental materials were taken from the Specimens Museum of the Shandong Jianzhu University (Jinan, China).

**Table 1:** Material information of 24 rosewood species in the experiment

ID	Latin name	Wood type	Place of origin	Species/genus
1	<i>Pterocarpus santalinus</i> L.f.	Diffuse-porous	India	Papilionaceae
2	<i>Pterocarpus erinaceus</i>	Diffuse-porous	Africa	Papilionaceae
3	<i>Pterocarpus indicus</i>	Diffuse-porous	Indonesia	Papilionaceae
4	<i>Pterocarpus macrocarpus</i>	Diffuse-porous	Myanmar	Papilionaceae
5	<i>Dalbergia odorifera</i> T. Chen	Diffuse-porous/semi-ring porous wood	Hainan	Papilionaceae
6	<i>Dalbergia cultrata</i>	Diffuse-porous	Myanmar	Papilionaceae
7	<i>Dalbergia latifolia</i>	Diffuse-porous	Indonesia	Papilionaceae
8	<i>Dalbergia louvelii</i> R.Vig	Diffuse-porous	Madagascar	Papilionaceae
9	<i>Dalbergia melanoxyton</i>	Diffuse-porous	Tanzania	Papilionaceae
10	<i>Dalbergia stevensonii</i> Standl	semi-ring porous wood	Mexico	Papilionaceae
11	<i>Dalbergia bariensis</i> Pierre	Diffuse-porous	Laos	Papilionaceae
12	<i>Dalbergia cearensis</i> Ducke	Diffuse-porous	Brazil	Papilionaceae
13	<i>Dalbergia cochinchinensis</i> Pierre	Diffuse-porous	Laos	Papilionaceae
14	<i>Dalbergia frutescens</i> Var.tomentosa (Vogel) Benth	Diffuse-porous/semi-ring porous wood	Brazil	Papilionaceae
15	<i>Dalbergia granadillo</i> Pittier	Diffuse- porous	Mexico	Papilionaceae
16	<i>Dalbergia oliveri</i> Prain	Diffuse-porous/semi-ring porous wood	Wah City	Papilionaceae
17	<i>Dalbergia retusa</i> Hemsl	Diffuse-porous	Nicaragua	Papilionaceae
18	<i>Millettia laurenlii</i> De Wild	Diffuse-porous	Congo	Papilionaceae
19	<i>Millettia leucantha</i>	Diffuse-porous	Myanmar	Papilionaceae
20	<i>senna siamea</i>	Diffuse-porous	Myanmar	Caesalpiaceae
21	<i>Diospyros ebenum</i> Koenig	Diffuse-porous	Philippines	Ebenaceae
22	<i>Diospyros crassiflora</i>	Diffuse-porous	Cameroon	Ebenaceae
23	<i>Diospyros celebica</i>	Diffuse-porous	Sulawesi	Ebenaceae
24	<i>Diospyros philippinensis</i> Gurke	Diffuse-porous	Philippines	Ebenaceae

## 2.2 Dataset Construction

The wood was prepared into small specimens with a size of 5 mm × 5 mm × 20 mm and scanned by micro-CT (SKYSCAN1272). The specimens and equipment are shown in Fig. 1. The specimen was put into the micro-CT and fixed well. The scanning parameters were set to 50 kV, 200 mA, and the scanning resolution was 2 μm. The height of the specimen was set to about 10 mm, and the scanning time of each specimen was about 100 min. After the scanned specimens were reconstructed, images of cross sections, radial sections and tangential sections of wood could be obtained.

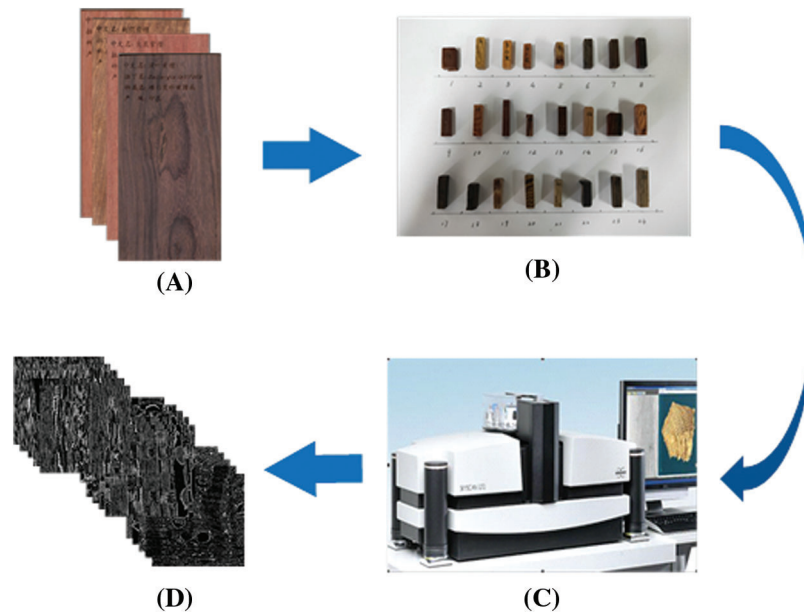


**Figure 1:** Acquisition of micro images. (A) is original samples; (B) is scanning specimens; (C) is scanning equipment; (D) are micro images

There were 3000 images collected from each specimen, including 1000 images from the cross sections, 1000 images from the radial sections and 1000 images from the tangential sections. 100 images were randomly selected from each section and then randomly cut into sub-images with the size of  $500 \text{ px} \times 500 \text{ px}$ , which were used to construct the data set of wood three sections. Ultimately, 7200 micro images of wood were obtained, which came from 2400 images of each tangential section, radial sections section and tangential section of 24 tree species, for the training of ELM and BP neural network.

### 3 Method

#### 3.1 Feature Extraction

The logical binary pattern (*LBP*), uniform *LBP* ( $LBP_{P,R}^{u2}$ ), rotation invariant *LBP* ( $LBP_{P,R}^r$ ), rotation invariant uniform *LBP* ( $LBP_{P,R}^{riu2}$ ), local configuration pattern (*LCP*), 5 forms were to extract cross sections, radial sections and tangential sections of 24 wood species in this paper.

##### 3.1.1 *LBP* (Logical Binary Pattern)

*LBP* is a kind of operator to describe texture features, which was first proposed by Ojala et al. [22]. The original *LBP* operator is defined as a  $3 \times 3$  window, taking the center pixel of the window as the threshold and comparing it with the gray value of the 8 adjacent pixels. If the surrounding pixel is larger than the center pixel, it is marked as 1; otherwise, it is marked as 0. Eight points produce an 8-bit unsigned number, the *LBP* value of the form, which represents the texture information for the expected region. By replacing the square neighborhood with a circular neighborhood, the  $3 \times 3$  window of the classical *LBP* operator is extended to an arbitrary range of radius *R*. Circular *LBP* operator was proposed by Ojala et al. [23] in 2002. The mathematical expression of circular *LBP* operator is:

$$w(x) = \begin{cases} 1, & x \geq 0 \\ 0, & x < 0 \end{cases} \quad (1)$$

$$LBP_{P,R} = \sum_{i=0}^{P-1} w(g_i - g_c) \cdot 2^i \quad (2)$$

### 3.1.2 Uniform LBP

Uniform pattern is defined as LBP binary pattern, there are two jumps from 0 to 1 or from 1 to 0 at most. For example, 00001000 (two jumps, 0-1,1-0) and 00110000 (0-1,1-0) are uniform patterns. The formula of uniform pattern is as follows:

$$U(LBP_{P,R}) = |s(g_{p-1} - g_c) - s(g_0 - g_c)| + \sum_{i=1}^{P-1} |s(g_i - g_c) - s(g_{i-1} - g_c)| \quad (3)$$

When  $U \leq 2$  is in uniform pattern, it is expressed by  $LBP_{P,R}^{u2}$ . The feature dimension of texture features is reduced from  $2^P$  to  $P(P-1) + 2$ , and the types of binary modes are greatly reduced.

### 3.1.3 Rotation Invariant LBP

In order to make the LBP operator rotation invariant, Ojala et al. [23] proposed the concept of Rotation Invariant LBP. By rotating clockwise for one revolution according to the number of adjacent points, different binary codes can be obtained in the circular region. The rotation invariant property is described by the LBP value of the region, which is the minimum value in binary coding. The mathematical expressions are as follows:

$$LBP_{P,R}^{ri} = \min\{ROR(LBP_{P,R}, i), i = 0, 1, \dots, P-1\} \quad (4)$$

$ROR(x, i)$  is a function used to rotate, performing a circular bit-wise right shift on the  $x$ -bit binary number by  $i$  times.

### 3.1.4 Rotation Invariant Uniform LBP

Combining the rotation invariant LBP with the uniform pattern to obtain the Rotation invariant uniform LBP, which has better effect. It is represented by symbols  $LBP_{P,R}^{riu2}$ , and the expression is as follows:

$$LBP_{P,R}^{riu2} = \begin{cases} \sum_{i=0}^{P-1} s(g_i - g_c), & U(LBP_{P,R}) \leq 2 \\ P + 1 & \end{cases} \quad (5)$$

### 3.1.5 LCP (Local Configuration Pattern)

*LCP* model is used to describe the texture features of images. The algorithm consists of two parts: the traditional *LBP* texture feature and the microscopic structure feature. By combining the above two features, the image information expression of *LCP* model is more detailed [24]. *LBP* features are calculated by comparing the gray values of a pixel with those of neighboring points. The structure of the *LCP* is illustrated in Fig. 2.

In addition to *LBP* and its deformation features, *GLCM* (Gray Level Co-Occurrence Matrix) and Tamura features were extracted, respectively. *GLCM* feature is a common method to describe texture by researching the spatial correlation characteristics of image gray scale. Inspired by human visual perception and psychological research, six Tamura texture features have been proposed. Roughness, contrast, directivity, linearity, regularity and roughness are used to extract texture features of micro images in this paper.

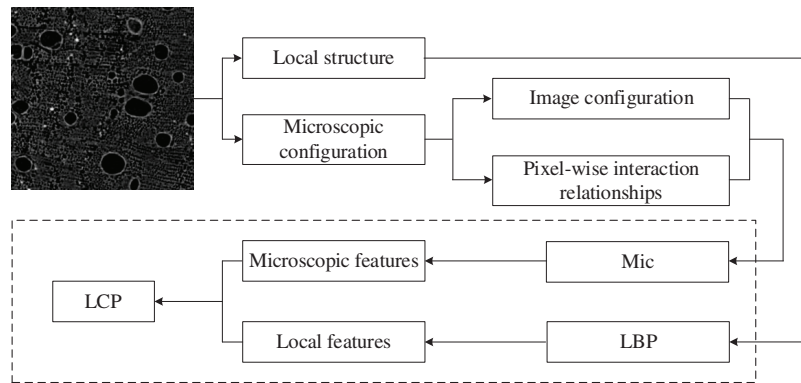


**Figure 2:** A structure for feature extraction of LCP

### 3.2 PCA Principle and Feature Dimension Reduction

PCA (Principal Component Analysis) is a method to build a new feature set by combining the existing features to remove redundant features and reduce dimension. On the premise of better representing the original feature data, PCA essentially projects the sample data in high-dimensional space to low-dimensional space through linear transformation [25,26].

Assuming that there are  $N$  training images with the size of  $m \times n$  and the dimension of  $M = m \times n$ , the  $i$ -th image is represented by one-dimensional vector  $x_i$ , and  $N$  images can be represented as a training set  $X$ , as shown in formula (6):

$$X = \{x_1, x_2, \dots, x_N\} \quad (6)$$

The mean value of training samples  $\bar{x}$  can be expressed as (7):

$$\bar{x} = \frac{1}{N} \sum_{i=1}^N x_i \quad (7)$$

The difference between the training sample and the sample mean  $A = [x_1 - \bar{x}, x_2 - \bar{x}, \dots, x_N - \bar{x}]$ , the covariance matrix of the training sample set  $S$ , as (8) shows

$$S = \sum_{i=1}^N (x_i - \bar{x})(x_i - \bar{x})^T = AA^T \quad (8)$$

Obviously, the covariance matrix  $S$  is a real symmetric matrix, and the existence of matrix  $u$  makes  $S$  similar to the diagonal matrix, as shown in (9):

$$u^T S u = [u_1, u_2, \dots, u_k, \dots, u_M]^T S [u_1, u_2, \dots, u_k, \dots, u_M] = \begin{pmatrix} \lambda_1 & \dots & 0 \\ \vdots & & \vdots \\ 0 & \dots & \lambda_M \end{pmatrix} \quad (9)$$

Among them  $\lambda_1, \lambda_2, \dots, \lambda_M$  is the eigenvalue of covariance matrix  $S$ .  $u_1, u_2, \dots, u_M$  is the feature vector corresponding to the covariance matrix. Selection of principal components and the  $M$  feature values are arranged in order of size. Select the feature vector corresponding to the first  $k$  maximum feature values, that is the final projection data. The selected projection data features are combined with classifiers for recognition and classification.

### 3.3 Feature Fusion

For features ( $LBP$ ,  $LCP$ ,  $LBP_{P,R}^{ri}$  and  $LBP_{P,R}^{iu2}$ ) with more feature dimensions, the classification takes a long time. Therefore, after PCA dimensionality reduction, the projection data corresponding to the first 20 maximum eigenvalues is selected as the feature vector. After dimensionality reduction  $LBP$ ,  $LCP$ ,  $LBP_{P,R}^{ri}$  and  $LBP_{P,R}^{iu2}$  are fused with  $GLCM$  and  $Tamura$  features respectively to obtain  $LBP+G+T$ ,  $LCP+G+T$ ,  $LBP_{P,R}^{iu2}+G+T$  and  $LBP_{P,R}^{ri}+G+T$  fused features, as shown in Fig. 3. Because the feature dimension of  $LBP_{P,R}^{iu2}$  is only 10 dimensions and the feature dimension is less, dimension reduction is not carried out, and it is directly fused with the features of  $GLCM$  and  $Tamura$  to obtain  $LBP_{P,R}^{iu2}+G+T$ .

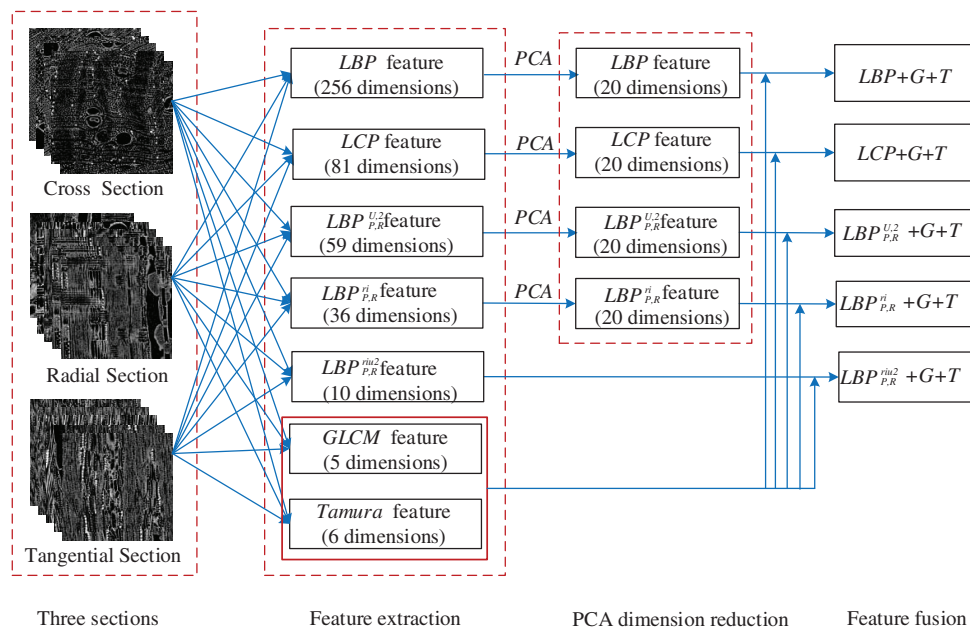


Figure 3: PCA reduction dimension and feature fusion

### 3.4 Classification

In view of the cross sections, radial sections and tangential sections of each species in 24 kinds of rosewood, five feature fusion methods ( $LBP+G+T$ ,  $LCP+G+T$ ,  $LBP_{P,R}^{iu2}+G+T$ ,  $LBP_{P,R}^{ri}+G+T$  and  $LBP_{P,R}^{iu2}+G+T$ ) were used to obtain the features. ELM and BP neural network were used to classify the five fusion features obtained from each section. The data of training set and test set were 70% and 30%, respectively.

ELM is a new single hidden layer feedforward neural network proposed by Huang [27]. This algorithm does not require complex iterative calculation, which is straightforward to select parameters, rapid learning speed and good generalization performance [17]. By setting the number of hidden layer nodes, the network can generate a unique optimal solution through random input weights and hidden layer bias. For the five fused features, the number of nodes in the hidden layer is set as 50 in this paper.

The BP neural network consists of three layers: the input layer, the hidden layer and the output layer. The hyperbolic tangent function  $\tanh$  was used as the transfer function from the input layer to the hidden layer, and the purelin function was used as the transfer function from the hidden layer to the output layer. The training times were 1000 and the learning rate was 0.01, the error rate of the training target was 0.00001, the momentum parameter was 0.01, and the minimum performance gradient was  $1e-6$ .

## 4 Results and Analysis

The classification results of five fused features by ELM and BP neural network were given in this paper, and the classification performance of the two classifiers in cross sections, radial sections and tangential sections were compared.

#### 4.1 Classification of ELM

Five fused features ( $LBP+G+T$ ,  $LCP+G+T$ ,  $LBP_{P,R}^{u2}+G+T$ ,  $LBP_{P,R}^{ri}+G+T$  and  $LBP_{P,R}^{riu2}+G+T$ ) were combined with ELM to classify cross sections, radial sections and tangential sections. From Fig. 4, it is known that all the five features exhibit the highest classification accuracy of the cross sections, followed by the radial sections, and ultimately the tangential sections. The classification accuracy of  $LBP_{P,R}^{ri}+G+T$  is low in three sections, and the accuracy of cross sections, radial sections and tangential sections are 96.67%, 88.75% and 73.19%. The classification effect of  $LBP_{P,R}^{u2}+G+T$  feature is the best, and the accuracy of cross sections, radial sections and tangential sections is 100%, 97.63% and 94.72%.

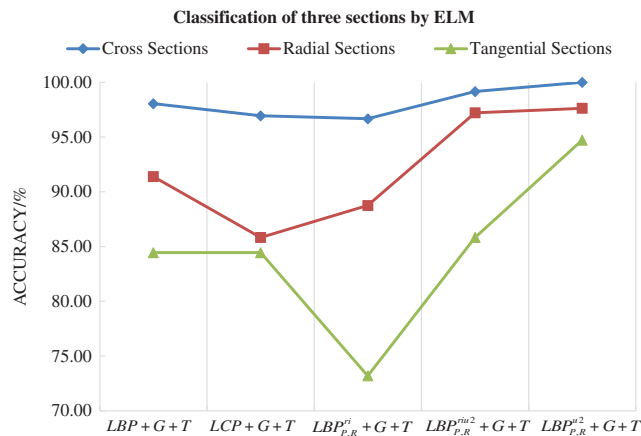


Figure 4: Classification of three sections by ELM

#### 4.2 BP Neural Network Classification

Five fused features ( $LBP+G+T$ ,  $LCP+G+T$ ,  $LBP_{P,R}^{u2}+G+T$ ,  $LBP_{P,R}^{ri}+G+T$  and  $LBP_{P,R}^{riu2}+G+T$ ) were combined with BP neural network to classify the cross sections, radial sections and tangential sections. As can be seen from Fig. 5, the five fused features show that the classification accuracy of cross sections is the highest, followed by radial sections, and finally tangential sections.  $LBP_{P,R}^{ri}+G+T$  has low accuracy in the classification of three sections, and the accuracy of cross, radial and tangential sections is 94.86%, 86.67% and 80.97%. The classification effect of feature  $LBP_{P,R}^{u2}+G+T$  is the best, and the accuracy of cross, radial and tangential sections is 99.17%, 94.86%, 89.02%.

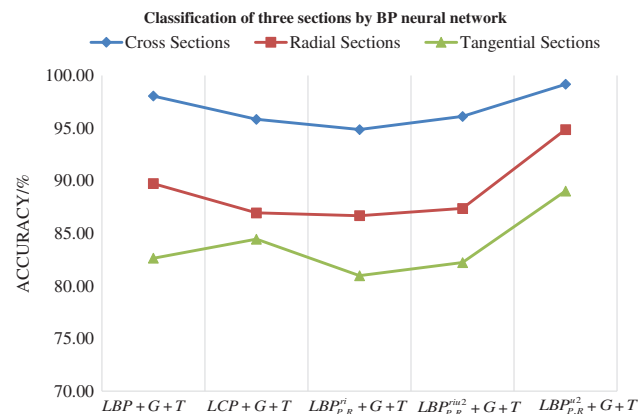
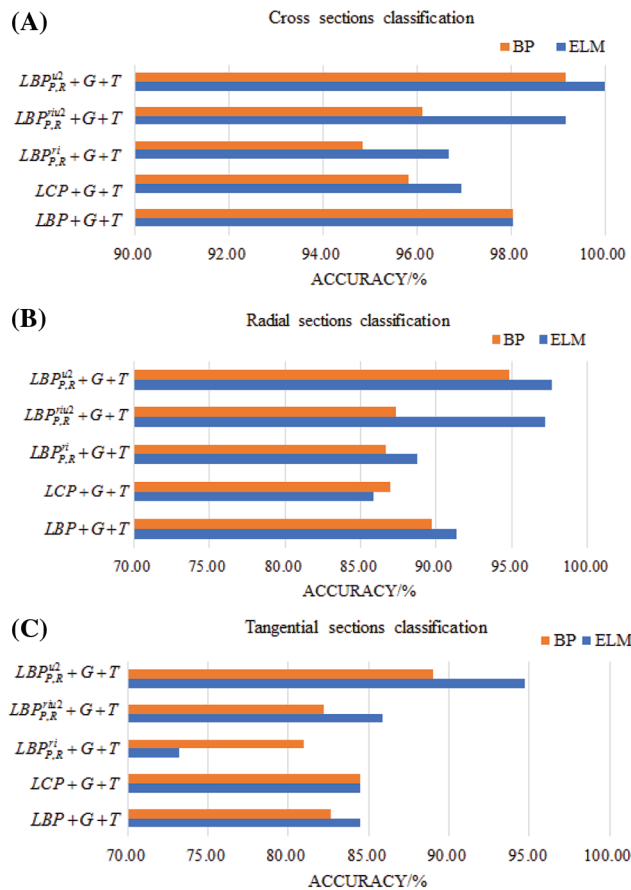


Figure 5: Classification of three sections by BP neural network

### 4.3 Comparison of ELM and BP Neural Network Results

In order to evaluate the performance of the two classifiers, the classification results of ELM and BP neural network in three sections are compared, as shown in Fig. 6. In the classification of cross sections as shown in (A), the classification accuracy of ELM is higher than that of BP neural network. In the classification of radial sections as shown in (B), except for  $LCP+G+T$  features, the classification accuracy of other four features ELM is higher than that of BP neural network. In the classification of tangential sections as shown in (C), except for  $LBP_{P,R}^{ri}+G+T$  features, the classification accuracy of the other four features ELM is higher than or equal to that of BP neural network. Consequently, in the classification of three sections, the classification effect of ELM for the fused features ( $LBP_{P,R}^{u2}+G+T$ ,  $LBP_{P,R}^{ri2}+G+T$ ,  $LBP+G+T$ ) is better than that of BP neural network.



**Figure 6:** Compared the classification results of ELM and BP neural network in three sections, (A) is Cross sections classification accuracy; (B) is radial sections classification accuracy; (C) is tangential sections classification accuracy

As can be seen from Table 2, among the five fusion features classified by ELM and BP neural network,  $LBP_{P,R}^{u2}+G+T$  has the best effect. Combined with BP neural network classification, the classification accuracy of cross sections, radial sections and tangential sections are 99.17%, 94.86% and 89.02%, respectively, and the time taken is 230.82, 236.15 and 215.53 s. After ELM classification, the classification accuracy of cross sections, radial sections and tangential sections is improved by 0.83%, 2.77% and 5.7%, respectively, and the classification time is only 0.72, 0.70 and 0.68 s. ELM classifier not only reduces operation time, but also improves classification accuracy.

**Table 2:** Classification results of ELM and BP neural network

Classifier	Feature fusion	Cross sections		Radial sections		Tangential sections	
		Accuracy (%)	Time (s)	Accuracy (%)	Time (s)	Accuracy (%)	Time (s)
ELM	$LBP+G+T$	98.05	0.72	91.39	0.73	84.44	0.71
	$LCP+G+T$	96.94	0.65	85.83	0.71	84.44	0.72
	$LBP_{P,R}^i+G+T$	96.67	0.68	88.75	0.70	73.19	0.73
	$LBP_{P,R}^{iu2}+G+T$	99.16	0.69	97.22	0.65	85.83	0.64
	$LBP_{P,R}^{u2}+G+T$	100.00	0.72	97.63	0.70	94.72	0.68
BP neural network	$LBP+G+T$	98.05	229.63	89.72	242.23	82.63	235.46
	$LCP+G+T$	95.83	200.02	86.94	268.25	84.44	255.95
	$LBP_{P,R}^i+G+T$	94.86	206.34	86.67	236.15	80.97	261.74
	$LBP_{P,R}^{iu2}+G+T$	96.11	112.22	87.36	177.01	82.22	145.27
	$LBP_{P,R}^{u2}+G+T$	99.17	230.82	94.86	236.15	89.02	215.53

## 5 Conclusions

1. In the classification of three sections using five fused texture features ( $LBP+G+T$ ,  $LCP+G+T$ ,  $LBP_{P,R}^{u2}+G+T$ ,  $LBP_{P,R}^i+G+T$  and  $LBP_{P,R}^{iu2}+G+T$ ) combined with ELM and BP neural network, the classification accuracy of the cross sections was the highest, followed by the radial sections, and ultimately the tangential sections. The classification accuracy of the cross sections is higher than that of the radial and tangential sections, indicating that the cross sections contain a large amount of texture information of wood micro images, which should be considered as an important factor for classification. Meanwhile, the radial and tangential sections also contain a large amount of micro image information, which can be used as an important reference basis for classification.
2. Among the five texture feature fusion methods,  $LBP_{P,R}^{u2}+G+T$  method shows excellent classification performance in ELM and BP neural network classification. The classification effect of  $LBP_{P,R}^{u2}+G+T$  combined with ELM is the best. The classification accuracy of cross sections, radial sections and tangential sections reaches 100%, 97.63% and 94.72% respectively, which is 0.83%, 2.77% and 5.70% higher than that of BP neural network. The classification running time of ELM is less than 1 s, and the classification efficiency is high. In conclusion, the  $LBP_{P,R}^{u2}+G+T$  method combined with ELM can be a quick and accurate classifier, providing an efficient and feasible classification method of rosewood.

**Funding Statement:** The Natural Science Foundation of Shandong Province, China (Grant No. ZR2020QC174). The Application of Computed Tomography (CT) Scanning Technology to Damage Detection of Timber Frames of Architectural Heritage. The Taishan Scholar Project of Shandong Province, China (Grant No. 2015162).

**Conflicts of Interest:** The authors declare that they have no conflicts of interest to report regarding the present study.

## References

1. Barmpoutis, P., Dimitropoulos, K., Barboutis, I., Grammalidis, N., Lefakis, P. (2017). Wood species recognition through multidimensional texture analysis. *Computers and Electronics in Agriculture*, 144(4), 241–248. DOI 10.1016/j.compag.2017.12.011.
2. Jahanbanifard, M., Beckers, V., Koch, G., Beeckman, H., Gravendeel, B. et al. (2020). Description and evolution of wood anatomical characters in the ebony wood genus *Diospyros* and its close relatives (Ebenaceae): A first step towards combatting illegal logging. *IAWA Journal*, 41(4), 577–619. DOI 10.1163/22941932-bja10040.
3. IAWA Committee (2004). IAWA list of microscopic features for softwood identification. *IAWA Journal*, 25(1), 1–70. DOI 10.1163/22941932-90000349.
4. Wheeler, E. A. (1989). IAWA list of microscopic features for hardwood identification. *IAWA Journal*, 10(3), 219–332.
5. Helmling, S., Olbrich, A., Heinz, I., Koch, G. (2018). Atlas of vessel elements. *IAWA Journal*, 39(3), 249–352. DOI 10.1163/22941932-20180202.
6. Kamal, K., Qayyum, R., Mathavan, S., Zafar, T. (2017). Wood defects classification using laws texture energy measures and supervised learning approach. *Advanced Engineering Informatics*, 34, 125–135. DOI 10.1016/j.aei.2017.09.007.
7. Stepanova, A. V., Vasilyeva, N. A. (2021). Wood identification of an ancient Greek coffin from the Bosporan Kingdom. *IAWA Journal*, 42(2), 209–215. DOI 10.1163/22941932-bja10048.
8. Yusof, R., Rosli, N. R., Khalid, M. (2010). Using gabor filters as image multiplier for tropical wood species recognition system. *IEEE 2010 12th International Conference on Computer Modelling and Simulation*, pp. 289–294. Cambridge, UK.
9. Yan, M. Z., Wang, H. Y., Wu, Y. Y., Cao, X. X., Xu, H. L. (2021). Detection of chlorophyll content of *Epipremnum aureum* based on fusion of spectrum and texture features. *Journal of Nanjing Agricultural University*, 44(3), 568–575. DOI 10.7685/jnau.2020060131.
10. Ahmad, K., Khan, K., Al-Fuqaha, A. (2020). Intelligent fusion of deep features for improved waste classification. *IEEE Access*, 8(99), 96495–96504. DOI 10.1109/ACCESS.2020.2995681.
11. Zhao, P., Dou, G., Chen, G. S. (2014). Wood species identification using feature-level fusion scheme. *Optik*, 125(3), 1144–1148. DOI 10.1016/j.ijleo.2013.07.124.
12. Wang, C. K., Zhao, P. (2020). Wood species recognition using hyper-spectral images not sensitive to illumination variation. *Journal of Infrared, Millimeter, and Terahertz Waves*, 39(1), 72–85. DOI 10.11972/j.issn.1001-9014.2020.01.011.
13. Qing, Y., Zeng, Y., Li, Y., Huang, G. B. (2020). Deep and wide feature based extreme learning machine for image classification. *Neurocomputing*, 412(1–3), 426–436. DOI 10.1016/j.neucom.2020.06.110.
14. Tang, J., Deng, C., Huang, G. B. (2015). Compressed-domain ship detection on spaceborne optical image using deep neural network and extreme learning machine. *IEEE Transactions on Geoscience and Remote Sensing*, 53(3), 1174–1185. DOI 10.1109/TGRS.2014.2335751.
15. Hu, X. H., Zeng, Y. J., Xu, X., Zhou, S. H., Liu, L. (2021). Robust semi-supervised classification based on data augmented online ELM with deep features. *Knowledge-Based Systems*, 229(7), 107307. DOI 10.1016/j.knsys.2021.107307.
16. Zabala-Blanco, D., Mora, M., Hernandez-Garcia, R., Barrientos, R. J. (2020). The extreme learning machine algorithm for classifying fingerprints. *IEEE Computer Society*, 2020, 1–8. DOI 10.1109/SCCC51225.2020.9281232.
17. Xiao, W., Yang, J. H., Fang, H. Y., Zhuang, J. T., Ku, Y. D. (2019). A robust classification algorithm for separation of construction waste using NIR hyperspectral system. *Waste Management*, 90, 1–9. DOI 10.1016/j.wasman.2019.04.036.
18. Yang, Y., Zhou, X., Liu, Y. (2020). Wood defect detection based on depth extreme learning machine. *Applied Sciences*, 10(21), 7488. DOI 10.3390/app10217488.
19. Zhang, W. Y. (2015). *Research and application of near infrared spectroscopy to the discrimination of rare woods (Master Thesis)*. Zhejiang Agriculture Forestry University.

20. Zhao, Y., Han, J. C., Wang, C. K. (2021). Wood species classification with microscopic hyper-spectral imaging based on I-BGLAM. *Texture and Spectral Fusion*, 41(2), 599–605. DOI 10.3964/j.issn.1000-0593(2021)02-0599-07.
21. Xiang, D., Chen, Y., Chen, G. S. (2015). Wood texture classification algorithm based on LBP. *Journal of Fujian Forestry Science and Technology*, 42(4), 57–63. DOI 10.13428/j.cnki.fjlk.2015.04.012.
22. Ojala, T., Matti, P., Topi, M. (2013). A generalized local binary pattern operator for multiresolution gray scale and rotation invariant texture classification. *Lecture Notes in Computer Science*, (1), 399–408. DOI 10.1007/3-540-44732-6-41.
23. Ojala, T., Pietikainen, M., Maenpaa, T. (2002). Multiresolution gray-scale and rotation invariant texture classification with local binary patterns. *IEEE Transactions on Pattern Analysis and Machine Intelligence*, 24(7), 971–987. DOI 10.1109/TPAMI.2002.1017623.
24. Guo, Y., Zhao, G., Pietikäinen, M. (2011). Texture classification using a linear configuration model based descriptor. *Proceedings of the British Machine Vision Conference*, pp. 119.1–119.10. BMVA Press. DOI 10.5244/C.25.119.
25. Dong, E. Z., Wei, K. X., Yu, X., Feng, Q. (2017). A model recognition recognition algorithm integrating PCA into LBP feature dimension reduction. *Computer Engineering and Science*, 39(2), 359–363. DOI 10.3969/j.issn.1007-130X.2017.02.021.
26. Erick, A., Okeyo, G. O., Kimwele, M. W. (2021). Feature selection for classification using principal component analysis and information gain. *Expert Systems with Applications*, 174, 114765. DOI 10.1016/j.eswa.2021.114765.
27. Huang G. B. (2014). An insight into extreme learning machines: random neurons, random features and kernels. *Cognitive Computation*, 6(3), 376–390. DOI 10.1007/s12559-014-9255-2.